

COMPUTATIONAL FLUID DYNAMICS MODEL OF THE VENTILATION AIR FLOW FOR A PROTECTIVE ENVIRONMENT ROOM

Mohd Hazzah Ahmad Siron^a, Md Amin Md Nor^{b*}

^aHVAC&R Section, Universiti Kuala Lumpur, Malaysia France Institute, Bangi, 43600 Selangor, Malaysia

^bAutomotive Engineering Section, Universiti Kuala Lumpur, Malaysia France Institute, Bangi, 43600 Selangor, Malaysia

Article history

Received

2 August 2021

Received in revised form

10 August 2023

Accepted

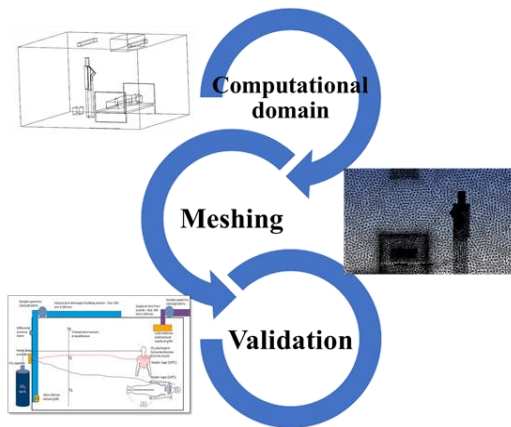
6 September 2023

Published Online

20 December 2023

*Corresponding author
mdamin@unikl.edu.my

Graphical abstract



Abstract

The outbreak of infectious diseases in the healthcare environment has prompted the need to study the efficacy of patients' protection inside a protective environment (PE) room. The main objective of this study is to develop a computational fluid dynamics model for a PE room. The development involved the selection of a turbulence equation and an optimum finite volume size. Prior to selecting the optimum finite volume size, grid convergence test was carried out on the model. Subsequently, the model was validated with a set of experimental data for the selection of the right turbulence equation. The results revealed that the optimum element size is 0.06 m with the realizable k-epsilon turbulence equation as a suitable equation for the room's air flow. The resultant model has laid an important foundation for future simulation studies on the PE room in any healthcare setting.

Keywords: Protective environment room, computational fluid dynamics, validation, grid convergence index, turbulence equation

Abstrak

Penularan penyakit berjangkit dalam persekitaran penjagaan kesihatan telah mendorong keperluan untuk mengkaji keberkesanan perlindungan pesakit di dalam bilik persekitaran perlindungan (PE). Objektif utama kajian ini adalah untuk membangunkan model perkomputeran dinamik bendalir untuk bilik PE. Pembangunan ini melibatkan pemilihan persamaan gelora dan ukuran isi padu terhingga optimum. Sebelum memilih ukuran isi padu terhingga optimum, ujian penumpuan bergrid dilakukan terhadap model. Selepas itu, model itu disahkan dengan satu set data eksperimen untuk pemilihan persamaan gelora yang tepat. Hasil kajian menunjukkan bahawa ukuran elemen optimum ialah 0.06 m dengan persamaan gelora k-epsilon realisasi sebagai persamaan yang sesuai untuk aliran udara di dalam bilik tersebut. Model yang dihasilkan ini telah meletakkan landasan penting untuk kajian simulasi di masa hadapan mengenai bilik PE di mana-mana persekitaran penjagaan kesihatan.

Kata kunci: Bilik persekitaran perlindungan, perkomputeran dinamik bendalir, pengesahan, ujian penumpuan bergrid, persamaan gelora

© 2024 Penerbit UTM Press. All rights reserved

1.0 INTRODUCTION

The outbreak of airborne infectious diseases has been rampant, such as Ebola in the Republic of Congo [1], measles resurgence in the USA [2], multidrug-resistance *Campylobacter* linked to puppies in the USA [3], leptospirosis in the tropical climate [4], as well as re-emergence of avian influenza A in China [5]. Furthermore, the outbreak of COVID-19 in China [6] and the rest of the world [7] has further raised the issue of mechanical ventilated air as an important element during aerosol transmission, which may be of either short or long range between the infected and exposed persons [8].

Due to its highly infectious nature, the pandemic has created anxiety, depression [9], and mental health [10] among Asian countries, and infected patients can potentially transmit these pathogens to healthcare workers, which are further transported via the mechanical ventilation system throughout the hospital environment [11]. There have been reports on the increased infection in surgical wards in Malaysian hospitals [12]. Another study conducted in a teaching hospital in the East Coast of Malaysia identified that the infection occurred in operating theatres [13]. Meanwhile, the study by Phoon *et al.*, showed that the infection was detected in isolation rooms [14].

In order to protect immunosuppressed patients from infected healthcare workers, there is a need to re-assess the ventilation system inside a protective environment (PE) room. Experiments have been the main research technique for indoor ventilation studies. However, three major disadvantages are associated with experiments [15]. The first disadvantage is that measurements can only be taken at only a few points. The second disadvantage is current visualisation techniques, such as particle imaging velocimetry, cannot provide a quantitative evaluation of cross-infection risks. The third disadvantage is the long response time of the measuring instrument, which is of the order of 1 to 10 s for tracer gas measurement. Thus, due to these circumstances, most of the experiments are conducted under steady-state conditions, and the data obtained are the time average data. Furthermore, the installed measuring instrument might render some flow disturbances. In addition, experimental apparatuses, such as breathing thermal manikins, are quite expensive [15].

As an alternative, numerical modelling using computational fluid dynamics (CFD) has become an integral part of ventilation studies [16]. CFD can provide detailed information in a very high temporal resolution on the flow and concentration parameters in the computational domain of a building ventilation system [17] and it contains no flow disturbances due to measuring instruments [15]. For ventilation research, CFD can be utilised at a much cheaper cost in comparison with experiments [18].

The main objective of this paper is to develop a computational model for a positive pressure isolation

room or a PE room. The model is based on a steady-state condition with a healthcare worker stands on the left-hand side of the bed while the immunosuppressed patient (IP) lies on the bed.

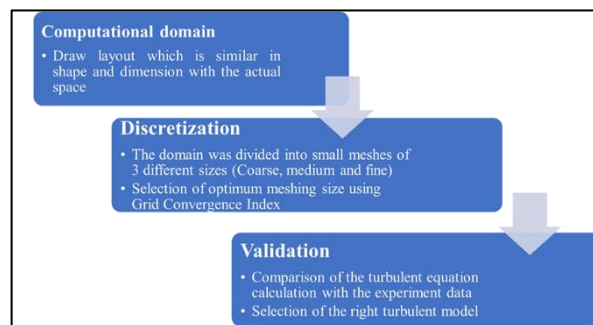


Figure 1 Flow path of CFD modelling

2.0 METHODOLOGY

The flow path of CFD modelling is shown in Figure 1. Prior to the development of the computational model, an experiment was conducted in a mock-up positive pressure PE room.

2.1 Experimental Set-up

A mock-up PE room with the dimensions of 3.66 m × 3.36 m × 2.4 m was erected, located in Universiti Kuala Lumpur, Malaysia France Institute. A unidirectional supply air grille (1.2 m × 0.6 m) was installed above the patient's bed, whereas an exhaust air grille (0.225 m × 0.225 m) was located at 1.7 m in the x-direction and 0.4 m in the z-direction (Figure 2).

Both supply and exhaust air grilles were connected to a galvanised iron ductwork and further equipped with variable speed fans. Then, a fan coil unit was installed inside the room to maintain a background temperature of 20.2 ± 0.75 °C. Three hot wire anemometers (Testo Model 0635 1025) were used to measure the air temperature with an accuracy of ± 0.3 °C and located as per Figure 3. A differential pressure gauge (Dwyer Instrument) was utilised to measure the pressure differences between the PE room and its immediate space. A carbon dioxide (CO₂) sensor (Testo Model 0632 1535) with an accuracy of ± 75 ppm was placed at the exhaust air grille.

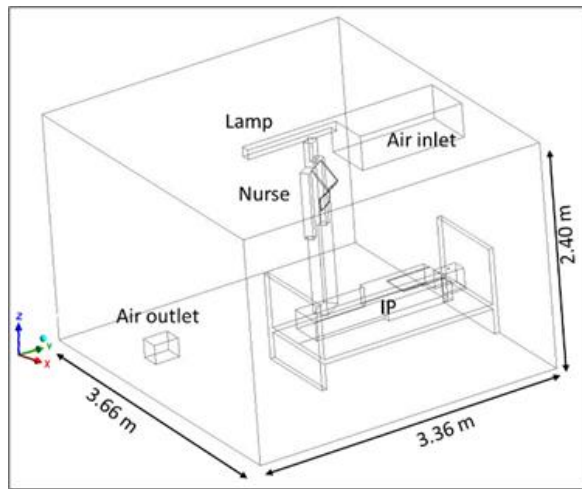


Figure 1 Dimensions of PE room and locations of supply air grille, exhaust air grille, HCW manikin, and IP manikin

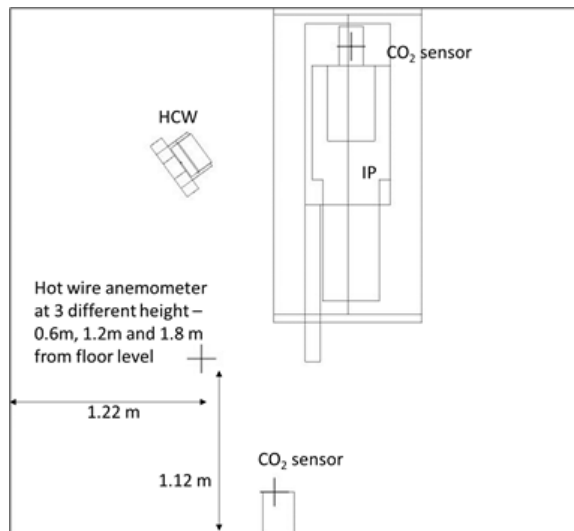


Figure 2 Locations of velocity, temperature, and CO₂ sensors

Two manikins were manipulated as the healthcare worker (HCW) and immunosuppressed patient (IP) and arranged as shown in Figure 3. The source-contaminated manikin (i.e., HCW) is of a typical Malaysian female adult's height, depicting a nurse, while the exposed manikin (i.e., IP) is of a typical Malaysian male adult's height, depicting an IP. The HCW manikin was in a standing position, whereas the IP manikin was in a supine position. The upper-front part of both manikins was covered with electric heaters to simulate human skin temperature at 34 °C [19] with an accuracy of ± 1 °C. Meanwhile, the power supply to the electric heaters was regulated using Red Lion model T16 controllers. The HCW manikin exhaled CO₂ gas through its mouth at the flow rate of 7 L/min using a 9.5 mm flexible hose with the 'jet' direction parallel to the floor. Mouth exhalation was specifically chosen due to higher horizontal propagation distance compared to nose breathing [20]. Another CO₂ sensor (Testo Model 0632 1535) was placed at a distance of 0.005 m from the face of the IP manikin. Melikov and Kaczmarczyk [21]

reported that air sampling at the upper lip at a distance less than 0.01 m from the face ensures that the measurement of pollution concentration is consistent with those measured in the inhaled air. Each probe was subsequently connected to a multi-function measuring instrument (Testo Model 435-2).

2.2 Experimental Procedure

The air supply into the environment protective room was set to 12 ACH, whereas the differential pressure between the room and its immediate space was maintained at $+2.5 \pm 1.25$ Pa. This approach prevents any indoor CO₂ from the neighbouring workshop from entering the chamber and tampering with the resulting CO₂ data collection at the exposed manikin. Furthermore, the air temperature within the room was set at 20.2 ± 0.75 °C by allowing the air conditioning unit to operate continuously during the experiment. Meanwhile, the heaters on both manikins were maintained at 34 ± 1 °C. Once the CO₂ concentration had reached a constant concentration, the tracer gas (CO₂) was released at a rate of 7 L/min continuously for 2 h. The air velocity, temperature, and CO₂ concentration were recorded at a 6-second interval. While the tracer gas was being released, the wall, floor, and ceiling temperatures were recorded using an infrared thermometer (Raytek Minitemp) at an accuracy of ± 2 °C. The experiment was repeated three times on different days.

2.3 Computational Domain

The computation domain was modelled using commercial computational fluid dynamics (CFD) software ANSYS Fluent 19.0 code. Meanwhile, the calculations for the air flow and spatial distribution of the tracer gas were generated using Reynolds-averaged Navier-Stokes equation.

The computational domain is similar to the experimental set-up, as shown in Figure 4.

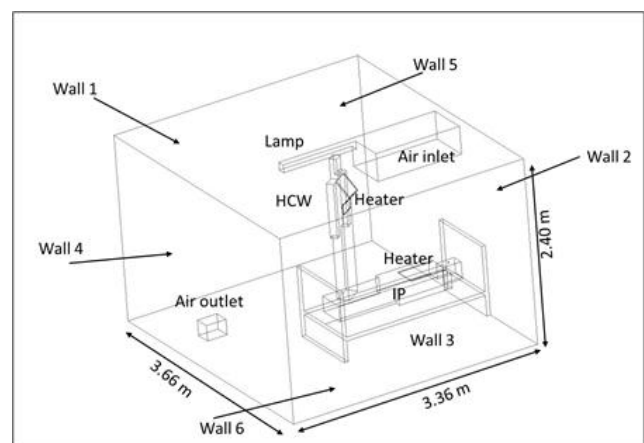


Figure 4 Computational domain

The size of the domain was 3.66 m \times 3.36 m \times 2.4 m, which consisted of two manikins. The geometries for

both manikins were drawn as simplified shapes as the study focused on the global flow condition only [22, 23]. This simplification requires fewer elements, thus reducing the calculation time [24]. The manikin bodies were subjected to heat similar to the experiment.

A unidirectional air inlet with the size of 1.15 m x 0.54 m was located above the exposed manikin, whereas an air outlet with the size of 0.199 m x 0.199 m was located at a low level. Their locations are in accordance with the ASHRAE Standard 170 recommendation on the 'Protective Environment' room [25].

All furniture, excluding the patient's bed, were excluded from the domain to simplify the calculation. This is as per Chen and Srebric [26], whereby a validation using simple geometry is acceptable and offers better computational reliability. The boundary conditions were set similar to the experimental conditions, as listed in Table 1.

Table 1 Boundary conditions for computational validation

Item	Type	Boundary conditions
1	Wall 1	20.8 °C
2	Wall 2	20.2 °C
3	Wall 3	21.0 °C
4	Wall 4	21.4 °C
5	Wall 5	20.6 °C
6	Wall 6	19.2 °C
7	Lamp	25.0 °C
8	Standing manikin's heater	34.2 °C
9	Lying manikin's heater	33.6 °C
10	Inlet air	17.6 °C 1% turbulence intensity 0.128 kg/s
11	CO ₂ inlet	4 Pa gauge pressure 20.2 °C 1% turbulence intensity, 0.000212 kg/s – constant exhalation
12	Operating pressure	100,860 Pa

2.4 Computational Grids

The accuracy of the computational calculation is also dependent on the discretisation scheme of the mesh generation [27]. Due to various geometries present in the domain, a tetrahedral type of grid element was selected. The mesh generation was optimised by performing a grid convergence index (GCI), as proposed by Roache [28] on three element quantities. The purpose of GCI is to verify an optimum grid element quantity so that further refinement of the grid will not substantially alter the computational solutions [29]. Therefore, Equation 1 was used for GCI [28]:

$$GCI = F_s \times \left| \frac{f_2 - f_1}{1 - r_{12}^p} \right| \tag{1}$$

Where F_s is the safety factor, f_1 and f_2 are any solutions for fine and coarse grids, respectively, r_{12} is a

grid refinement ratio, and p is the formal order of accuracy. The formal order of accuracy is given by Equation 2 [27]:

$$p = \frac{\ln\left(\frac{f_3 - f_2}{f_2 - f_1}\right)}{\ln r_{12}} \tag{2}$$

Where f_3 is the solution of the coarser grid.

The GCI was performed on 1.8 million, 2.4 million, and 3.7 million cells. This has resulted in the values of GCI (CO₂ mass fraction at IP's nose) of 0.003% between 1.8 million and 2.4 million, and 0.001% between 2.4 million and 3.7 million cells accordingly. Thus, the 2.4 million cells with a grid size of 0.06 m were selected as the domain to optimise the computing time.

2.5 Turbulence Model and Computational Method

K-epsilon turbulence models were considered in this study due to their wide applicability in flow situations and the need for less computational demand [27,30,31]. Three types of k-epsilon models were subsequently selected: the standard k-epsilon [32], re-normalisation group (RNG) k-epsilon [33], and realizable (Real) k-epsilon [34] models. For the solution method, a coupled scheme was used with second-order upwind for the momentum, CO₂, and energy, whereas first-order upwind was chosen for turbulent kinetic energy and dissipation rate. As for the solver, pressure-based steady-state solver was chosen and 1,000 iterations was performed.

3.0 RESULTS AND DISCUSSION

3.1 Validation

Figure 5 displays a comparison of average CO₂ mass fraction between the experimental measurements and simulated results, whereas Figure 6 shows the plot of temperatures between the experimental measurements and simulated data.

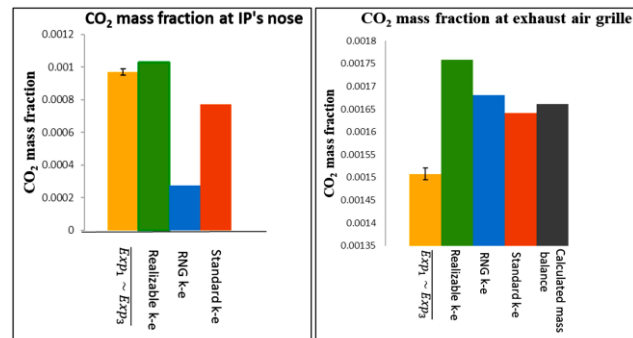


Figure 5 CO₂ mass fraction (a) near the IP's nose and (b) at the exhaust air grille. The error bar shows 2 standard deviations

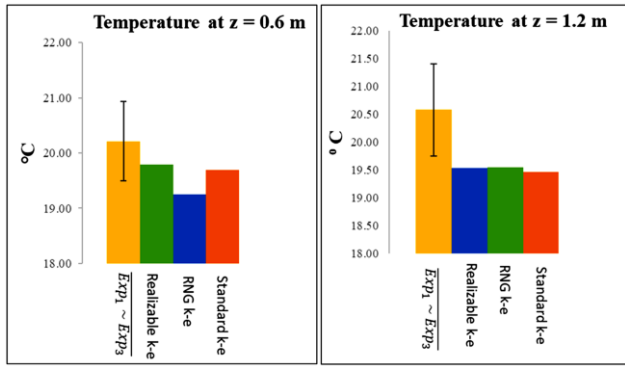


Figure 6 Space temperatures between experimental measurements and simulated data at (a) 0.6 m height, (b) 1.2 m height, (c) 1.8 m height, and (d) at the exhaust air grille. The error bar shows 2 standard deviations

As per Figure 5(a), the realizable k-epsilon model calculation was found to be in close agreement with the experimental value, with a difference of 6.1% compared to the standard k-epsilon (20.4%) and RNG k-epsilon (71.5%) models. However, Figure 5(b) indicates that the realizable k-epsilon model showed the highest difference (16.7%) compared to the RNG k-epsilon (11.5%) and standard k-epsilon (8.9%) models. This is primarily due to exfiltrated air from the room as the room was maintained at +2.5 Pa. Meanwhile, a comparison of the calculated CO₂ mass balance indicated that the error associated with the realizable k-epsilon model was only 5.9%.

Figure 6 shows that all computed temperatures are underestimated. However, the temperature variations between the measurement data and simulated data for all three height sensors and the exhaust air grille were found to be less than 6% for all turbulence models. At the height of 0.6 m, the real k-epsilon model displayed the lowest value of 2.1%, whereas at the height of 1.2 m, the real k-epsilon and RNG k-epsilon models obtained the lowest value of 5.0% each. Meanwhile, at the height of 1.8 m, the standard k-epsilon model recorded the lowest value of 1.7%, while at the exhaust air outlet, the real k-epsilon model achieved the lowest value of 3.4%.

All errors should be less than 10% [35] to be considered in good agreement with the model; hence, the realizable k-epsilon model was selected as the turbulence model for the investigation of simulation case studies. It has been proven to model the flow better than the standard k-epsilon model, consume less time [34], and produce good results for both high and low Reynolds number turbulent flow [36], including recirculation flow [37].

3.2 Comparison with Previous Studies

Figure 7 illustrates the velocity vectors of the inlet air from the laminar diffuser above the IP, indicating its unidirectional property, as per ASHRAE Standard 170 recommendations [25].

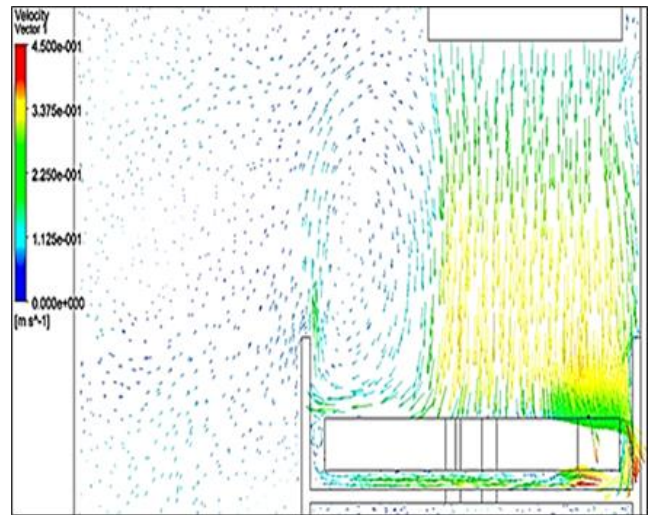


Figure 7 Inlet air flow vectors above the lying manikin

Meanwhile, Figure 8 displays the temperature contours at three different heights. The air temperature inside the room (i.e., 23 °C) was in the range of the ASHRAE Standard 170 recommendations [25], which is 21–24 °C.

Figure 9 shows a comparison of the temperature gradient between the standing manikin's chest and the experiment carried out by Licina *et al.*, [38] at a surrounding air temperature of 23 °C. The surface temperature of the HCW was set at 34 °C, while the manikin's surface temperature in the experiment was 32.6 °C. Therefore, the simulated temperature gradient is in good agreement with the experimental result.

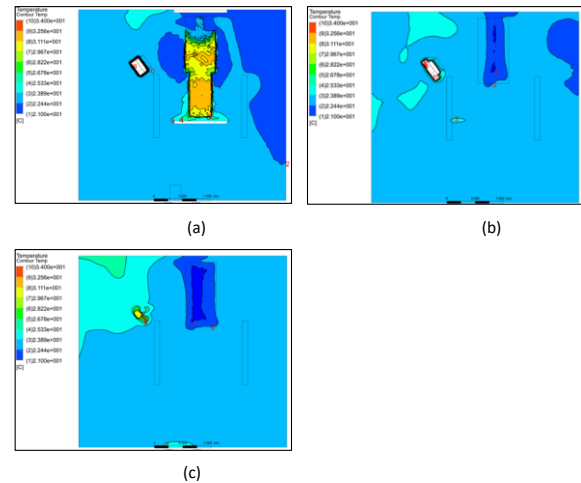


Figure 8 Temperature contours at (a) z = 0.6 m, (b) z = 1.2 m, and (c) z = 1.8 m

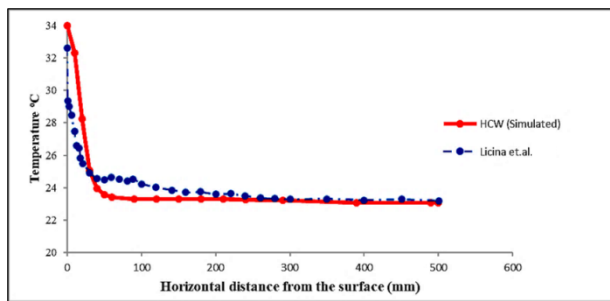


Figure 9 Temperature gradient between the simulated HCW's chest and the experiment carried out by Licina *et al.* [38]

The difference between the manikin's surface temperature of 34 °C and the room's air temperature has subsequently created a density gradient or thermal plume. Figure 10 shows the upward air flow vectors on the manikin's surface due to the thermal plume, whereby the upward air velocity was approximately 0.2–0.25 m/s. This finding is in agreement with several previous studies [39,40,41].

The upward exhalation flow from the standing manikin is depicted in Figure 11. It is evident that the upward flow of the exhalation is attributable to its lower density compared to the air density, as well as the influence of the thermal plume. The result obtained is also in support of several previous studies [42,43]. Therefore, this finding indicates that the correct density of exhalation is crucial for experiments involving a breathing thermal manikin.

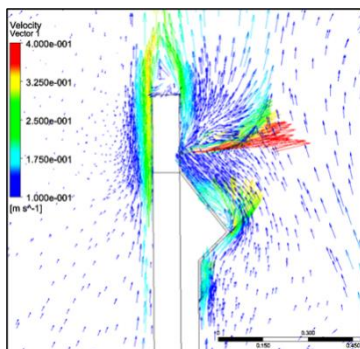


Figure 10 Upward air flow due to thermal plume

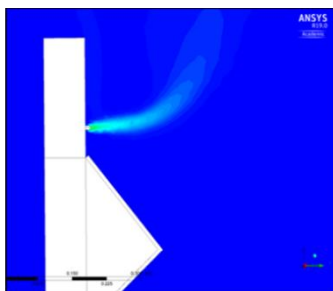


Figure 11 Upward exhalation flow from the standing manikin

4.0 CONCLUSION

The main aim of this paper is to develop a computational model of a PE room. The model was verified and validated using sets of experimental data collected from the experiments conducted in a mock PE room.

The computational model was discretised to an optimum tetrahedral finite element size of 0.06 m with the grid convergence index of 0.003%. The air flow behaviour was characterised by the realizable k-epsilon turbulence equation. The results of the calculation are less than 10% errors compared to the experimental data. The computational model is in agreement with previous research. The developed model has laid an important foundation for future simulation studies and improvement on the ventilation system inside a PE room.

Conflicts of Interest

The author(s) declare(s) that there is no conflict of interest regarding the publication of this paper.

Acknowledgement

The authors express their gratitude to Universiti Kuala Lumpur Malaysia France Institute, Malaysia, for funding this research. The authors also appreciate the assistance provided by Water Engineering and Conditioned Air section in allowing us to conduct the physical experiment and CFD simulation in their laboratories.

References

- [1] Green, A. 2018. Ebola Outbreak in the DR Congo: Lessons Learned. *Lancet*. 391(10135): 2096. Doi: [https://doi.org/10.1016/S0140-6736\(18\)31171-1](https://doi.org/10.1016/S0140-6736(18)31171-1).
- [2] Sarkar, A., A. Zlojutro, K. Khan, and L. Gardner. 2019. Measles Resurgence in the USA: How International Travel Compounds Vaccine Resistance. *Lancet Infectious Diseases*. 19(7): 684-686. Doi: [https://doi.org/10.1016/s1473-3099\(19\)30231-2](https://doi.org/10.1016/s1473-3099(19)30231-2).
- [3] Montgomery, M. P., Robertson, S., Koski, L., *et al.* 2018. Multidrug-Resistant *Campylobacter jejuni* Outbreak Linked to Puppy Exposure — United States, 2016–2018. *MMWR Morbidity and Mortality Weekly Report*. 67(37): 1032-1035. Doi: <http://dx.doi.org/10.15585/mmwr.mm6737a3>.
- [4] Lee, B., and E. Rose. 2018. Other Potentially Life-Threatening Conditions with Mucocutaneous Findings (Leptospirosis, Typhoid Fever, Dengue, Diphtheria, Murine Typhus). *Life-Threatening Rashes: An Illustrated, Practical Guide*. 319-347. Doi: https://doi.org/10.1007/978-3-319-75623-3_23.
- [5] Lu, Y., S. Landreth, A. Gaba, M. Hlasny, G. Liu, Y. Huang, and Y. Zhou. 2019. In Vivo Characterization of Avian Influenza A (H5N1) and (H7N9) Viruses Isolated from Canadian Travelers. *Viruses*. 11(2): 193. Doi: <https://doi.org/10.3390/v11020193>.
- [6] Muralidar, S., S. V. Ambi, S. Sekaran, and U. M. Krishnan. 2020. The Emergence of COVID-19 as a Global Pandemic: Understanding the Epidemiology, Immune Response and Potential Therapeutic Targets of SARS-CoV-2. *Biochimie*. 179: 85-100.

- Doi: <https://dx.doi.org/10.1016%2Fj.biochi.2020.09.018>.
- [7] Keni, R., A. Alexander, P. G. Nayak, J. Mudgal, and K. Nandakumar. 2020. COVID-19: Emergence, Spread, Possible Treatments, and Global Burden. *Frontiers in Public Health*. 8: 216. Doi: <https://doi.org/10.3389/fpubh.2020.00216>.
- [8] Liu, L., Y. Li, P. V. Nielsen, J. Wei, and R. L. Jensen. 2017. Short-Range Airborne Transmission of Expiratory Droplets Between Two People. *Indoor Air*. 27(2): 452-462. Doi: <https://doi.org/10.1111/ina.12314>.
- [9] Leong Bin Abdullah, M. F. I., H. Ahmad Yusof, N. Mohd Shariff, R. Hani, N. F. Nisman, and K. S. Law. 2021. Depression and Anxiety in the Malaysian Urban Population and Their Association with Demographic Characteristics, Quality of Life, and the Emergence of the COVID-19 Pandemic. *Current Psychology*. 1-12. Doi: <https://doi.org/10.1007/s12144-021-01492-2>.
- [10] Wang, C., M. Tee, A. E. Roy et al. 2021. The Impact of COVID-19 Pandemic on Physical and Mental Health of Asians: A Study of Seven Middle-Income Countries in Asia. *PLOS ONE*. 16(2): e0246824. Doi: <https://doi.org/10.1371/journal.pone.0246824>.
- [11] Suleyman, G., G. Alangaden, and A. C. Bardossy. 2018. The Role of Environmental Contamination in the Transmission of Nosocomial Pathogens and Healthcare-Associated Infections. *Current Infectious Disease Reports*. 20(6): 12. Doi: <https://doi.org/10.1007/s11908-018-0620-2>.
- [12] Halain, A. A., K. L. Soh, A. Ibrahim, S. Japar, S. L. Ong, A. M. Sani, ... K. G. Soh. 2018. Nursing Workload in Relation to Nosocomial Infection in Public Hospital Intensive Care Unit, Malaysia. *Research Journal of Pharmacy and Technology*. 11(9): 3892-3896. Doi: <https://doi.org/10.5958/0974-360X.2018.00713.8>.
- [13] Khaidi, N. A. K. M., S. M. Anua, N. Mazlan, and S. N. Saud. 2021. The Presence of Microbial Air Contaminants in the Operating Theatre at a Teaching Hospital in East Coast Malaysia. *Open Biology Journal*. 9(1): 11-16. Doi: <http://dx.doi.org/10.2174/1874196702109010011>.
- [14] Ai, Z. and A. K. Melikov. 2018. Airborne Spread of Expiratory Droplet Nuclei Between the Occupants of Indoor Environments: A Review. *Indoor Air*. 28(4): 500-524. Doi: <https://doi.org/10.1111/ina.12465>.
- [15] Phoon, H. Y. P. H. Hussin, B. M. Hussain, S. Y. Lim, J. J. Woon, Y. X. Er, and K. L. Thong. 2018. Distribution, Genetic Diversity and Antimicrobial Resistance of Clinically Important Bacteria from the Environment of a Tertiary Hospital in Malaysia. *Journal of Global Antimicrobial Resistance*. 14(18): 132-140. Doi: <https://doi.org/10.1016/j.jgar.2018.02.022>.
- [16] Li, Y., and P. V. Nielsen. 2011. Commemorating 20 Years of Indoor Air: CFD and Ventilation Research. *Indoor Air*. 21(6): 442-453. Doi: <http://dx.doi.org/10.1111/j.1600-0668.2011.00723.x>.
- [17] Wang, H., and Z. (John) Zhai. 2016. Advances in Building Simulation and Computational Techniques: A Review between 1987 and 2014. *Energy and Buildings*. 128: 319-335. Doi: <http://dx.doi.org/10.1016/j.enbuild.2016.06.080>.
- [18] Nielsen, P. V. 2015. Fifty Years of CFD for Room Air Distribution. *Building and Environment*. 91: 78-90. Doi: <https://doi.org/10.1016/j.buildenv.2015.02.035>.
- [19] Gagge, A. P. and Y. Nishi. 2011. Heat Exchange Between Human Skin Surface and Thermal Environment. *Comprehensive Physiology*, Hoboken, NJ, USA: John Wiley & Sons. 69-92.
- [20] Xu, C., P. V. Nielsen, L. Liu, R. L. Jensen, and G. Gong. 2017. Human Exhalation Characterization with the Aid of Schlieren Imaging Technique. *Building and Environment*. 112: 190-199. Doi: <https://doi.org/10.1016/j.buildenv.2016.11.032>.
- [21] Melikov, A. and J. Kaczmarczyk. 2007. Measurement and Prediction of Indoor Air Quality Using a Breathing Thermal Manikin. *Indoor Air*. 17(1): 50-59. Doi: <https://doi.org/10.1111/j.1600-0668.2006.00451.x>.
- [22] Topp, C., P. Hesselholt, M. R. Trier, and P. V. Nielsen. 2003. Influence of Geometry of Thermal Manikins on Concentration Distribution and Personal Exposure. 2: 357-362.
- [23] Yan, Y., X. Li, and J. Tu. 2017. Effects of Manikin Model Simplification on CFD Predictions of Thermal Flow Field Around Human Bodies. *Indoor and Built Environment*. 26(9): 1185-1197. Doi: <https://doi.org/10.1177%2F1420326X16653500>
- [24] Mahyuddin, N., H. B. Awbi, and E. A. Essah. 2015. Computational Fluid Dynamics Modelling of the Air Movement in An Environmental Test Chamber with A Respiring Manikin. *Journal of Building Performance Simulation*. 8(5): 359-374. Doi: <https://doi.org/10.1080/19401493.2014.956672>.
- [25] ASHRAE. 2013. *ASHRAE Standard 170-2013, Ventilation of Health Care Facilities*. 2013th ed. Atlanta, GA: ASHRAE.
- [26] Chen, Q., and J. Srebric. 2002. A Procedure for Verification, Validation, and Reporting of Indoor Environment CFD Analyses. *HVAC&R Research*. 8(2): 201-216.
- [27] Awbi, H. B. 2005. *Ventilation of Buildings*. 2nd ed. London & New York: Taylor & Francis Group.
- [28] Roache, P. J. 1997. Quantification of Uncertainty in Computational Fluid Dynamics. *Annual Review of Fluid Mechanics*. 29(1): 123-160.
- [29] Sørensen, D. N. and P. V. Nielsen. 2003. Quality Control of Computational Fluid Dynamics in Indoor Environments. *Indoor Air*. 13(1): 2-17. <https://doi.org/10.1111/j.1600-0668.2003.00170.x>.
- [30] Launder, B. E., and D. B. Spalding. 1972. *Mathematical Models of Turbulence*. London: Academic Press.
- [31] Rodi, W. 2000. *Turbulence Models and Their Application in Hydraulics*. 3rd ed. London and New York: Taylor & Francis.
- [32] Launder, B. E., and D. B. Spalding. 1974. The Numerical Computation of Turbulent Flows. *Computer Methods in Applied Mechanics and Engineering*. 3(2): 269-289. Doi: [http://dx.doi.org/10.1016/0045-7825\(74\)90029-2](http://dx.doi.org/10.1016/0045-7825(74)90029-2).
- [33] Yakhot, V., S. A. Orszag, S. Thangam, T. B. Gatski, and C. G. Speziale. 1992. Development of Turbulence Models for Shear Flows by A Double Expansion Technique. *Physics of Fluids A: Fluid Dynamics*. 4(7): 1510-1520. Doi: <https://doi.org/10.1063/1.858424>.
- [34] Shih, T.-H., W. W. Liou, A. Shabbir, Z. Yang, and J. Zhu. 1995. A New $k-\epsilon$ eddy Viscosity Model for High Reynolds Number Turbulent Flows. *Computers & Fluids*. 24(3): 227-238. Doi: [https://doi.org/10.1016/0045-7930\(94\)00032-T](https://doi.org/10.1016/0045-7930(94)00032-T).
- [35] Zhang, Z., W. Zhang, Z. J. Zhai, and Q. Y. Chen. 2007. Evaluation of Various Turbulence Models in Predicting Airflow and Turbulence in Enclosed Environments by CFD: Part 2— Comparison with Experimental Data from Literature. *HVAC&R Research*. 13(6): 871-886. Doi: <https://doi.org/10.1080/10789669.2007.10391460>.
- [36] Antoun, S., N. Ghaddar, and K. Ghali. 2016. Coaxial Personalized Ventilation System and Window Performance for Human Thermal Comfort in Asymmetrical Environment. *Energy and Buildings*. 111: 253-266. Doi: <http://dx.doi.org/10.1016/j.enbuild.2015.11.030>.
- [37] Hussain, S., P. H. Oosthuizen, and A. Kalendar. 2012. Evaluation of Various Turbulence Models for the Prediction of the Airflow and Temperature Distributions in Atria. *Energy and Buildings*. 48: 18-28. Doi: <https://doi.org/10.1016/j.enbuild.2012.01.004>.
- [38] Licina, D., A. Melikov, C. Sekhar, and K. W. Tham. 2015. Air Temperature Investigation in Microenvironment Around a Human Body. *Building and Environment*. 92: 39-47. Doi: <https://doi.org/10.1016/j.buildenv.2015.04.014>.
- [39] Mundt, E. 1995. Displacement Ventilation Systems— Convection Flows and Temperature Gradients. *Building and Environment*. 30(1): 129-133. Doi: [http://doi.org/10.1016/0360-1323\(94\)e0002-9](http://doi.org/10.1016/0360-1323(94)e0002-9).
- [40] Yang, C., X. Yang, and B. Zhao. 2015. The Ventilation Needed to Control Thermal Plume and Particle Dispersion from Manikins in A Unidirectional Ventilated Protective Isolation Room. *Building Simulation*. 8(5): 551-565. Doi: <https://doi.org/10.1007/s12273-014-0227-6>.
- [41] Li, J., J. Liu, C. Wang, N. Jiang, and X. Cao. 2017. PIV Methods for Quantifying Human Thermal Plumes in A Cabin Environment Without Ventilation. *Journal of Visualization*. 20(3): 535-548. Doi: <http://dx.doi.org/10.1007/s12650-016-0404-4>.

- [42] Jiang N., S. Yao, L. Feng, H. Sun, and J. Liu. 2017. Experimental Study on Flow Behavior of Breathing Activity Produced by A Thermal Manikin. *Building and Environment*. 123: 200-210. Doi: <https://doi.org/10.1016/j.buildenv.2017.07.004>.
- [43] Chen, C., and B. Zhao. 2010. Some Questions on Dispersion of Human Exhaled Droplets in Ventilation Room: Answers from Numerical Investigation. *Indoor Air*. 20(2): 95-111. Doi: <https://doi.org/10.1111/j.1600-0668.2009.00626.x>.